Advanced trim-cut technique to visualize melt flow dynamics inside laser cutting kerfs

D. ArntzD. PetringU. JansenR. Poprawe

Citation: Journal of Laser Applications **29**, 022213 (2017); doi: 10.2351/1.4983261
View online: http://dx.doi.org/10.2351/1.4983261
View Table of Contents: http://lia.scitation.org/toc/jla/29/2
Published by the Laser Institute of America

Advanced trim-cut technique to visualize melt flow dynamics inside laser cutting kerfs

D. Arntz
Chair for Laser Technology LLT, RWTH Aachen University, Steinbachstr. 15, Aachen 52074, Germany

D. Petring
Fraunhofer Institute for Laser Technology ILT, Steinbachstr. 15, Aachen 52074, Germany

U. Jansen
Nonlinear Dynamics of Laser Processing NLD, RWTH Aachen University, Steinbachstr. 15, Aachen 52074, Germany

R. Poprawe
Chair for Laser Technology LLT, RWTH Aachen University, Steinbachstr. 15, Aachen 52074, Germany and Fraunhofer Institute for Laser Technology ILT, Steinbachstr. 15, Aachen 52074, Germany

(Received 28 March 2017; accepted for publication 28 March 2017; published 30 May 2017)

Instabilities of the laser cutting front cause loss of quality due to the formation of striations on the cut flank. The mechanisms of striation generation during laser cutting are still not yet fully understood. To visualize the laser cutting process, the trim-cut technique was invented many years ago and is being continuously improved by different authors in the last years as well as in current studies. During a trim-cut, the laser beam is moved in-parallel along an existing sheet flank and cuts off a stripe of less than a standard kerf width. The cutting front and the transition to the resultant cut flank are directly visible. Without additional measures, the cutting gas jet expands during trimming in the half space freed by the lack of a second cutting edge. To maintain a guided supersonic gas jet path along the melt film and simultaneously enable the *in-situ*-observation of the cutting kerf with high-speed imaging, the missing cut flank is simulated by a transparent substrate, e.g., made of synthetic fused silica. In this manner, the gas jet is guided between the transparent substrate and the opposite real cutting flank. In this paper, a comprehensive review about trim-cut studies from different authors is given. Furthermore, an automated trim-cut test bench with two fast, highly accurate *x*/*y*-tables and versatile control features, as well as recent research results on melt flow characteristics during laser cutting of 6 mm thick stainless steel with 1 μm wavelength and nitrogen assist gas, are presented. © *2017 Laser Institute of America*.
[http://dx.doi.org/10.2351/1.4983261]

Key words: laser cutting, high-speed imaging, 1 micron laser, process diagnostics

I. INTRODUCTION

High power laser cutting systems are mostly equipped with CO_2 ($\lambda = 10\,\mu$m) and fiber lasers ($\lambda = 1\,\mu$m), the latter meanwhile having a still growing market share over 50%.[1] However, particularly for thick section cutting of stainless steel, there are still drawbacks regarding the achievable cut quality with the recently established fiber lasers. Regardless of the laser type, the mechanisms of striation and dross generation are still not yet fully understood.

Understanding these mechanisms requires looking at the process in detail. High-speed video diagnostics provides temporally and spatially resolved insight into the dynamics of laser cutting. As a reason of the high aspect ratio between the sheet thickness and the kerf width (>10), the observability with off-axis or coaxial video diagnostics is limited and suffers from limited optical accessibility. Therefore, specific techniques are required to observe the cutting front and the transition to the resultant cut flank. To overcome these limitations, the trim-cut procedure can be used, in which the missing cut flank is replaced by a transparent substrate.

But even with such a transparent substrate, the trim-cut setup influences the cutting results, e.g., by changing the gas flow and beam propagation compared to the real cutting process. Nevertheless, this technique offers great potential for fundamental process analysis because of the direct observation of the interaction zone with a high temporal and spatial resolution.

The analysis of subprocesses such as the wave formation on the cutting front or the solidification process at the transition from the cutting front to the resultant cut flank is possible.

Therefore, it is valuable to further improve the trim-cut test procedure regarding operability and reliability and to increase the similarity between a trim cut and a normal cut (Table I).

II. LITERATURE REVIEW

In the late 1970s, the most simple approach of the trim-cut technique was invented by Arata *et al.*[2] In a so called edge cut procedure, they moved a CO_2 laser beam in-parallel along a mild steel flank and assured that the focal point was

TABLE I. Notation.

P	Laser power	(kW)
fps	Frames per second	(/s)
d_F	Focus diameter	(μm)
λ	Laser wavelength	(μm)
v_C	Cutting speed	(m/min)
z_F	Focus position	(mm)
v_{MAX}	Maximal velocity	(m/s)
a_{MAX}	Maximal acceleration	(m/s^2)
R_a	Arithmetic average roughness	(μm)
R_z	Mean roughness depth	(μm)

just on the edge of the workpiece surface so that they machined a thin slice from the workpiece. By using this technique, it was possible to film the motion of the melt flow on the cutting front with 1000 fps by using a high-speed camera, oriented perpendicular to the cut flank (Fig. 1).[2]

They observed that in the case of oxygen-assisted laser cutting, the reaction proceeds periodically and leaves striations for each cycle.

An essential improvement of this edge cut setup was made by Zefferer *et al*. in 1993.[3] In previous works, Petring[4] and Zefferer[5] analyzed the gas dynamical mechanism during laser cutting by Schlieren optical investigations which showed the differences between the propagation of a gas jet in a complete kerf and at an edge of a plate. Accordingly, they concluded that the expansion in the half space freed by the lack of a second cutting flank leads to an earlier boundary layer separation at the cutting front.

Therefore, Zefferer replaced the second cutting flank by a transparent glass sheet to guide the gas jet between the edge to be cut and the glass sheet. The destruction of the glass sheet by absorption of laser radiation ($\lambda = 10\,\mu$m) was prevented by a gap as narrow as possible between both elements. To compensate for gas flow asymmetry, the axis of the gas nozzle was adjusted in the center between the glass sheet and the cutting edge. Thus, the laser beam axis was decentred relative to the nozzle toward the cut edge. The height of the glass sheet was larger than the thickness of the metal sheet. So, the lower edge of the glass sheet was not levelled with the lower edge of the metal sheet.

Additionally, Zefferer used a focused light source to illuminate the interaction zone to reduce the contrast between the thermally radiating front and the already cold part of the flank. Before the edge cut, a precut was carried out, to ensure a parallel edge in the feed direction (Fig. 2).

With this setup, it was possible for the first time to visualize the ripple generation during laser beam fusion cutting

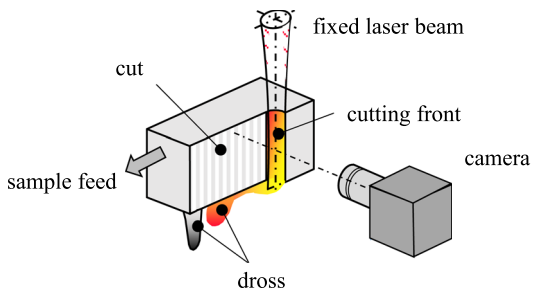

FIG. 1. Principle of trim-cut procedure invented by Arata *et al*.[2]

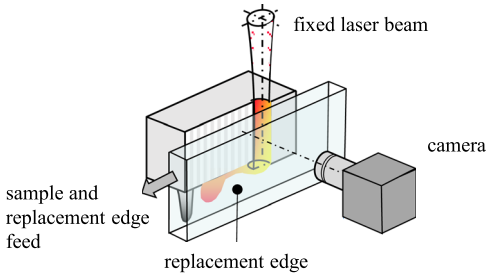

FIG. 2. Principle of trim-cut procedure modified by Zefferer *et al*.[3]

of metals. The material was 2 mm CrNi-steel cut with a speed of 2 m/min and a laser beam power of 1.2 kW and visualized with 1000 fps. The authors found out that ripples, which were visible as light and dark stripes, were formed in the area of transition from the cutting front to cut flank with an average time-constant of $T = 2$ ms.

In 2000, Fushimi *et al*.[6] used Arata's technique again to analyze gas assisted CO_2 laser cutting with different gases. They cut mild steel with a thickness of 4.4 mm at a laser power of 400–800 W by using oxygen and air as assist gases. They captured with 18 000 fps motions of molten metal with a periodic action in a time interval of every 2.22 and 18.6 ms, respectively. So, they presumed that the molten metal velocity is agile 2 m/s using oxygen assist gas, while it is 0.2 m/s with air.

In 2007, Yudin *et al*.[7–9] adopted the same approach as Zefferer and called it "trim-cut." Fusible metals with a low melting point and a thickness of 10 mm were cut instead of steel. Therefore, they used a CO_2 laser at a laser power of merely 300 W. In the same way as Zefferer *et al*.,[3] they fixed the replacement glass edge to the opposite of the metal surface with a gap of ~0.1 mm. They filled the gap with vacuum oil to avoid reflections of laser rays as well as metal film adhesion, which blocks visual access.

In their study, they observed the molten metal is transported both in the form of droplets and as film or rivulet, sliding down the walls of the kerf. They divided roughness formation during solidification into two types: stalactites and ripples, which indeed can also be formed on real cut flanks of the stainless steel (Fig. 3). They described that stalactites grow downward at a certain distance from the cutting front along the edge of the solidifying stream and are fed from this stream. Ripples are formed when there is a back and forth motion of the solidification front, e.g., due to the fluctuation in the molten stream width and are generated by sliding down the wall. Furthermore, they generate regular tiny ripples by modulation of laser power at 300 Hz.

Thus, the trim-cut procedure was successfully applied to laser cutting with inert gas cutting with low laser power. By using oxygen assist gas, the visual access to the cut kerf was blocked due to the layer of oil which burned and adhesion of the metal film to the glass.

To solve this problem, Ermolaev *et al*.[10] continued to improve the trim-cut technique by using an additional positioning table to move the replacement edge in the opposite feed direction as the metal sheet. They used this technique to reduce the thermal loads on the glass and furthermore to

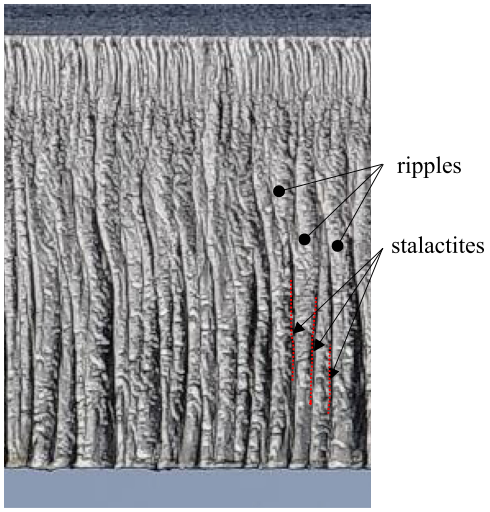

FIG. 3. Roughness formation on the cut flank (fiber laser @ 3 kW, 6 mm mild steel, v_C: 2.4 m/min, d_F: 200 μm, nozzle standoff 0.7 mm, z_F: −5 mm, cutting gas: nitrogen p: 20 bar).

remove defected glass areas instantly from the observation area (Fig. 4).

Thereby it was for the first time possible to visualize cutting of 12 mm thick mild steel with oxygen assist gas and 2 kW fiber laser power by using the trim-cut technique.

Petring presented the difference between CO_2 and fiber laser cutting with inert assist gas by using the trim-cut technique without moving glass for 4 mm stainless steel, successfully. The high speed videos show that the dynamically humping melt flow when using a fiber laser distinctively differs from the smooth and regular cutting front in case of a CO_2 laser with comparable beam power and geometry (Fig. 5).[11]

In Ref. 12, Hirano also used the trim-cut technique with moving replacement edge. Stainless steel with 3 and 5 mm thickness were cut with 4 kW fiber laser power with nitrogen assist gas pressure of 10–12 bar. An observation angle of the high speed video camera at 45° laterally to the cutting front was used to visualize interactions between melt flow in the central and side parts of the cutting front in an optimized manner.

They observed that not only the side flow but also the central flow of the melt influences the final striation pattern on kerf flanks. They identified a relationship between periodic striations with relatively low surface roughness and a stable central flow of the melt on the cutting front. Opposed to that effect, they showed that an unstable central flow leads

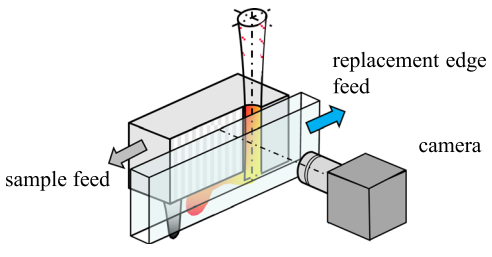

FIG. 4. Principle of trim-cut procedure improved by Ermolaev *et al.*[10]

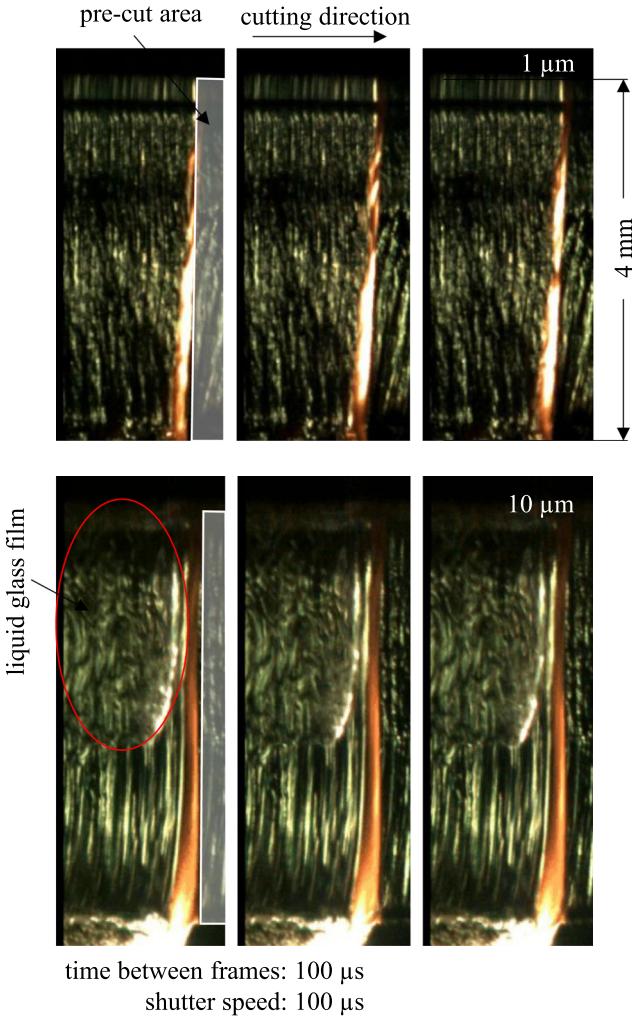

FIG. 5. High-speed video diagnostics of CO_2 and fiber laser cutting fronts in stainless steel.[11]

to chaotic interactions with melt accumulations, which results in a higher roughness of the cut flank.

Furthermore, a comprehensive study about laser cutting with fiber and CO_2 lasers using oxygen and inert gas assist during trim-cuts is given in Refs. 13 and 14. They used typical cutting parameters (CO_2: P: 4 kW, fiber laser: P: 2.4 kW, nozzle standoff 1 mm) and gave excellent examples of the successful application of the trim-cut technique with moving replacement edge. As in past studies,[10] they visualized the cutting procedure with 10 000 fps and used a high density light beam, collected by a reflector from a halogen lamp.

They confirmed the results of Petring[11] regarding the great influence of the type of wavelength on the character of the melt flow on the cutting front in cutting of stainless steel with nitrogen assist gas. As Petring they observed smooth melt flow with exact phase boundaries in the case of CO_2 radiation in contrast to highly unstable melt flow with multiple ejections to the cut flank in case of fiber laser radiation. They explain that in the case of 1 μm wavelengths as a reason of the ejection traces on the cut flank a high roughness is produced. For oxygen cutting, they observed that striations are formed by combustion cycles with a thin oxide layer and see a lower influence of the wavelength.[13,14]

The analysis of the fluid dynamics with the aid of a side positioned high speed camera is not only used in laser cutting but also in laser joining.

Tenner *et al.*[15] applied this setup to weld two zinc-coated steel plates (DX56) of 0.7 mm thickness in an overlap configuration. They attached a 1 mm thick borosilicate glass next to the metal sheets to flank the keyhole. Thus, they got a detailed look inside it. By using tracer particles to measure the fluid dynamics, they were able to resolve velocities inside the keyhole of up to several tens of meters per second.

III. ADVANCED TRIM-CUT PROCEDURE

The described studies show that the trim-cut procedure is suitable to visualize melt flow dynamics inside laser cutting kerfs with typical laser cutting parameters by the aid of high-speed video equipment.

For a systematic process analyses by means of the trim-cut procedure, it is reasonable to reassess the test procedure itself and design a test bench which takes the requirements of the test procedure into account at the best.

A. Preliminary trim-cut studies

To clarify the requirements of the advanced trim cut test bench, preliminary trim-cut studies with a fixed replacement edge were carried out.

1. Experimental trim-cut setup

The experiments were performed by using an *x/y* table (bidirectional repeatability $\pm 1\,\mu$m, straightness error $<5\,\mu$m). The x-axis was used for the feed direction, and the y-axis for the infeed direction. A redundant manual linear stage in the infeed direction was used for the positioning of the replacement edge. The axes-system was positioned below a cutting head.

The material used was stainless steel 1.4301. The samples with a thickness of 6 mm were milled to the dimensions of $60 \times 90\,\text{mm}^2$ with a maximum surface roughness of $R_a = 1.6\,\mu$m. Two dowel holes with a diameter of 3 mm were drilled into the samples to position the samples on the sample holder in parallel to the feed direction.

For the replacement edge, synthetic fused silica rods were used. The dimensions of the rods were $80 \times 5 \times 6\,\text{mm}^3$ (length, width, and height).

The experiments were carried out using an IPG YLC-4000 multimode fiber laser with a wavelength of 1070 nm and maximum output power of 4 kW. The fiber with a diameter of 100 μm was collimated and focused with a focal length of 120 mm and 290 mm, respectively. This configuration provides a focal diameter of 240 μm. The focus position was adjusted on the upper or on the bottom surface of the sample and a cutting speed of 2.5 m/min was used. A conical nozzle with a diameter of 5 mm was mounted and the stand-off distance of 0.7 mm was adjusted. The nitrogen assist gas was set to a pressure of 20 bar.

The trim-cuts were observed with the high speed camera Photron SA 5 at a frame rate of 100 kHz and a resolution of 128×376 px. To increase the dynamic range of the pictures, the thermally emitting interaction zone and the area beside that were additionally illuminated by two sideways positioned VCSEL-arrays (vertical-cavity surface-emitting laser) with an optical output of about 5 W each (Fig. 6).

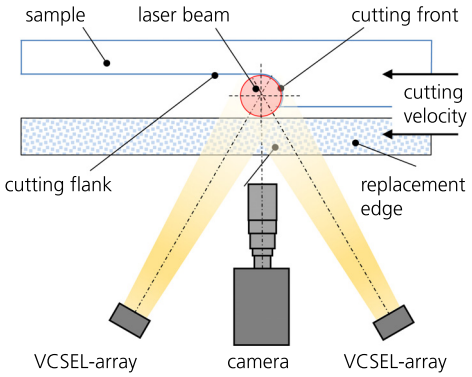

FIG. 6. Principle of experimental trim-cut setup.

2. Trim-cut parameter set

The trim-cut parameters are the trim-cut width and the distance between the replacement edge and the sample. For each parameter, two testing points were set. The set values for the trim-cut width were 50% (small) and 75% (wide) of the normal cut kerf width. The set values for the distance between replacement edge and sample were $<150\,\mu$m (small) and $>150\,\mu$m (wide) (Fig. 7).

Thus, four parameter sets were chosen to investigate the influence on the generation of the trim-cut flank.

There is a wide distance between the replacement edge and the sample with small or wide trim-cut width for parameter sets A and B, and a small distance between the replacement edge and the sample with a small or wide trim-cut width for parameter sets C and D.

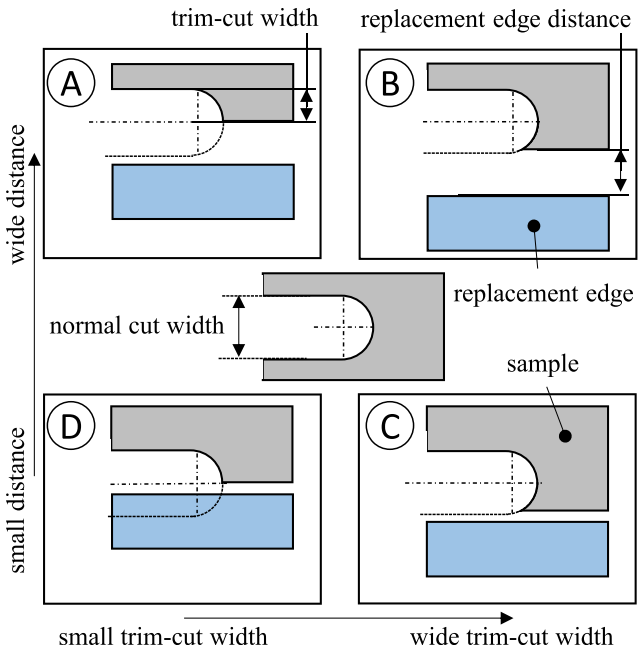

FIG. 7. Principle of trim-cut parameter sets.

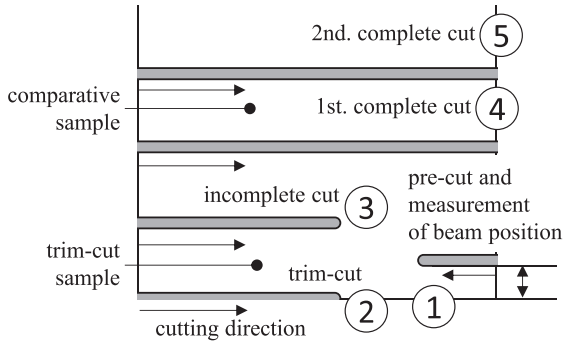

FIG. 8. Principle of trim-cut procedure.

3. Experimental trim-cut procedure

The sample and the replacement edge were positioned on the sample holder and on the replacement holder, respectively. The parallelism in the feed direction of both elements as well as the horizontal adjustment was verified and was set to a maximal deviation error $<10\,\mu$m. The kerf width and the position of the beam relative to the edge to be trimmed were determined by means of a side positioned pre-cut and measured with a mobile microscope (1). Thus, the trim-cut parameters were set by the knowledge of the beam position and the kerf width and the trim-cut was carried out (2). Thereafter, the trim-cut width and the distance between the sample and the replacement edge were measured with the mobile microscope. The procedure was completed with an incomplete (3) and two complete cuts (4, 5). In this manner, the trim-cut sample with two incomplete cuts and a sample with a left and right cut flank for comparative studies were available (Fig. 8).

4. Results concerning the trim-cut parameters

By using the described trim-cut procedure, the resulting cut front and cut flank structure of a trim-cut can be compared with a real cut under same conditions.

Figure 9 shows trim-cut and normal cut-flanks as well as kerf widths for the trim-cut parameter set A for the focus positions $z_F = 0$ mm and $z_F = -6$ mm. The striation pattern for $z_F = 0$ mm is on the normal cut flank minimal by angled in the lower part whereas it is nearly vertical on the trim-cut flank. This effect is more significant for $z_F = -6$ mm. For that case, the striation pattern of the normal flank can be distinctly separated into three parts, whereas only the upper part is similar to the trim-cut flank, which only shows a very weak three-sectioning (see red dotted line in Fig. 9). Although the three-sectioning is only weak, it is significant that this kind of striation pattern can be found even of the wide distance between the replacement edge and the sample. Furthermore, it is to note that the surface of a trim-cut flank is not necessarily worse than a normal cut flank.

Figure 10 shows the distances between the replacement edge and sample before and after the trim-cut for the trim-cut parameter sets C and D.

The distance after the trim-cut is larger for parameter set D, whereas it is the same for parameter set C. An

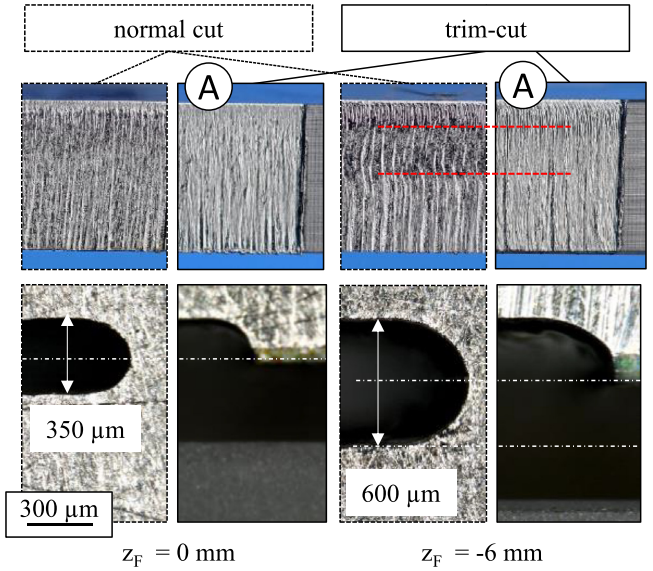

FIG. 9. Images of cut flanks and top views of normal cut kerfs (left) or trim-cuts (right) for parameter set A at different focus positions.

accumulation of melt can be found on the end position of the trim-cut flank for parameter set D in contrast to parameter set C (see red dotted ellipsis in Fig. 10). It can be assumed that the melt exerts a force on the replacement edge so that the distance gets larger. It is not clear whether the distance increases during the trim-cut or afterward when the melt resolidifies.

The trim-cut width for parameter set D is 150 μm instead of 175 μm. Thus, the trim-cut parameters deviate in some cases from the set values despite of a precise and careful experimental procedure. On the lower part of the trim-cut flank, an area of the original sample flank without resolidified melt can be identified (see red lined ellipsis in Fig. 10). As could have been expected, that the trim-cut width has to be at least or minimal wider than the half of the normal cut kerf to get a complete trim-cut.

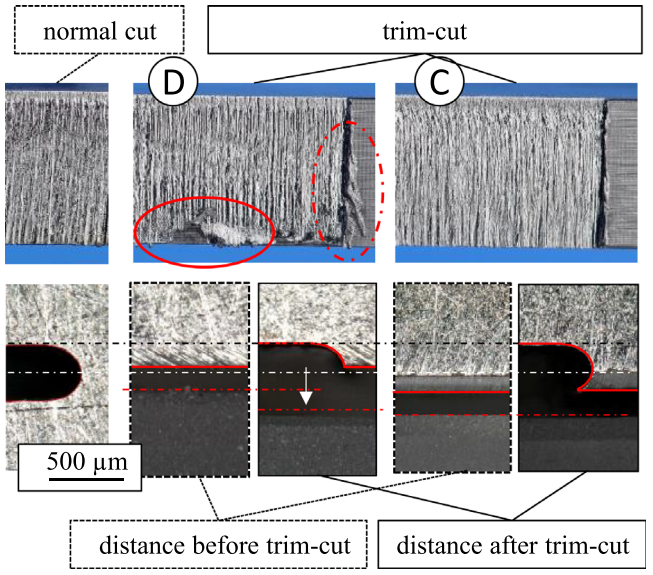

FIG. 10. Real cut (left) and offset before and after trim-cut between replacement edge and sample for trim-cut parameter set D and C (right), $z_F = 0$ mm.

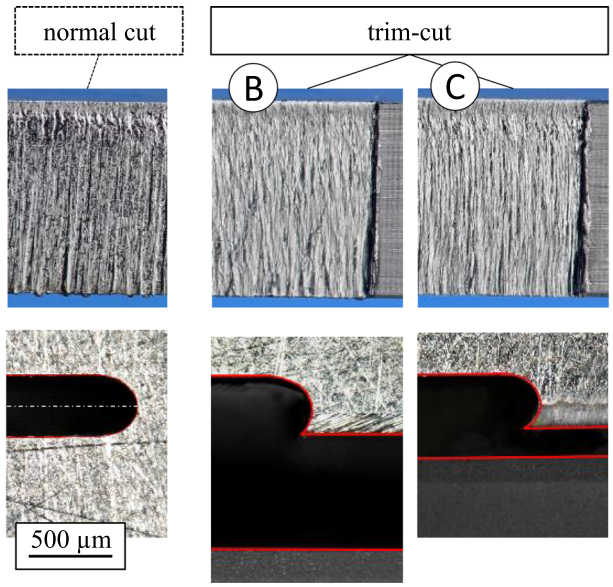

FIG. 11. Real cut (left) and trim-cuts with small and wide distance between replacement edge and sample, parameter set B and C, $z_F = 0$ mm.

Figure 11 shows the influence of a different distance between the replacement edge and the sample for nearly the same trim-cut width (trim-cut parameter sets B and C). A correlation between the upper part of the normal cut and the trim-cut flank occurs for parameter set C, in contrast to parameter set B, where the distance between the replacement edge and the sample is larger. Furthermore, the striation pattern is more regular and narrower in case C.

We conclude that a trim-cut width larger than half of the normal cut kerf and a further reduction of the replacement edge distance is worthwhile to increase the similarity of the trim-cut and the normal cut flanks.

5. Results concerning the trim-cut videos

A typical trimcut frame and the top view of the resulting trim-cut sample of trim-cut parameter set C with $z_F = -6$ mm are shown in Figure 12. The image shows the moving melt flow on the cutting front on the upper part and contamination of the replacement edge with resolidified melt in the lower part. A relative feed of the replacement edge seems reasonable to facilitate a permanent observation of the whole cutting front.

The bottom part of the frames are not analyzable due to the melt contamination of the replacement edge. Still, the frames are usable for analyzing the upper part of the kerf in particular, because it shows a significant similarity to the upper part of the corresponding normal cut flank. To define the maximum analyzable cut depths, a horizontal grayscale analysis of photographed cut flanks were performed to find peaks or rather striations. Therefore, a tool is developed using the Wolfram Mathematica system and its built-in FindPeaks algorithm. The input data for the algorithm is a 5 pixel (≈40 μm) vertical average of the gray scale input data (data range [0..1]). To filter out artifacts and incomplete striations, a threshold value of 0.5 is applied to the peaks found to detect a valid striation (Fig. 13).

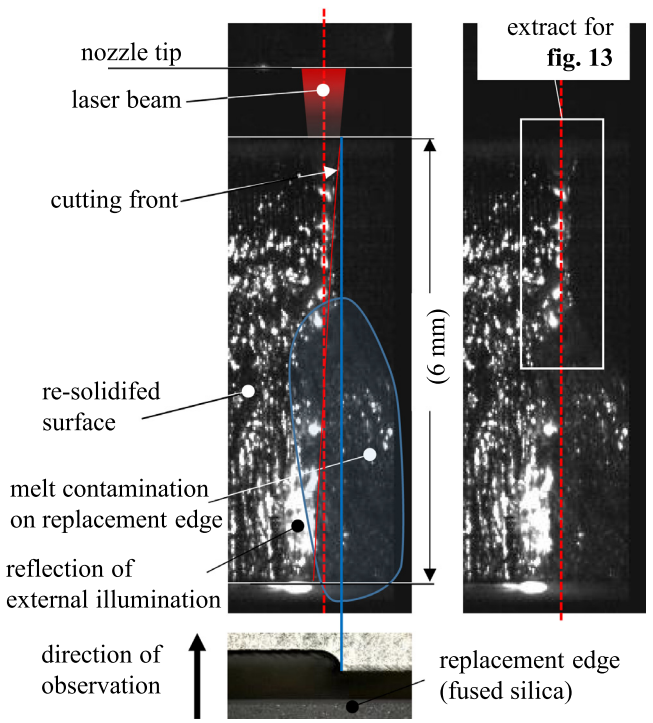

FIG. 12. Description of high speed image of trim-cut parameter set A, $z_F = -6$ mm.

Figure 14 shows the result of the grayscale analysis and thus the striations per mm for a trim cut and a normal cut for parameter set C. The values are nearly the same and in phase for cut depths to approximate 1 mm. Thus, we take it as a the maximum analyzable area for the following analyzation of trim-cut videos.

Figure 15 shows a false color extraction of a frame series for trim-cut parameter set C for $z_F = -6$ mm (cf. Fig. 12).

In that frame series it can be observed that even the melt flow on the top part of the cutting front seems to be deterministically chaotic, some dominant melt flows could be identified. The striation pattern on the cut-flank shows striations which are oriented forward to the cutting front. This pattern correlates with a melt stream on the left hand side (see white arrows in Fig. 15). Another dominant melt stream, which is oriented backwards, can be seen on the right hand side (see black arrows in Fig. 15). Both melt streams are flowing together and form vertical striations with an average

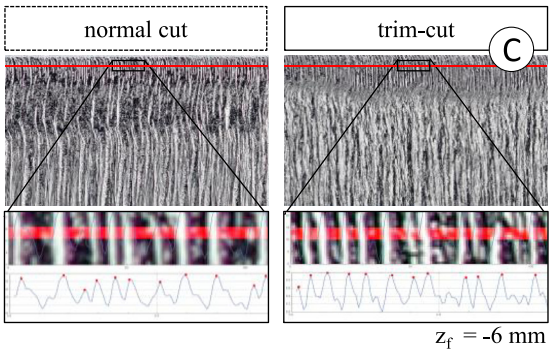

FIG. 13. Principle of horizontal grayscale analyses of striation pattern on cut flanks of normal cut kerfs (left) or trim-cuts (right) for parameter set C.

time-constant of $T = 1.8$ ms (for orientation, see red arrows in Fig. 15). It is to note that this is nearly the same value as Zefferer[3] had shown in 1993.

B. Automated trim-cut test bench

The preliminary studies show the importance of reproducible and accurate experimental conditions for an adequate performance of systematic trim-cut test series. Therefore, an automated trim-cut test bench has been engineered which takes the following aspects into account:

- Accurate and reproducible positioning of trim-cut sample and replacement edge.
- Low parallel error in the feed direction.
- Equipment for exact positioning and measuring of trim-cut and replacement edge and trim-cut width, respectively.
- Low speed fluctuation in feed and infeed directions.
- Accessibility for the high speed camera and illumination equipment.

1. Mechanical construction

The engineered trim-cut test bench is equipped with two *x*/*y* tables, each with a feed and infeed axes: One for the sample (X, Y) and one for the replacement edge (x, y). The feed directions (X, x) are the cutting direction and the direction of the moving replacement edge, respectively, both with a movement range of 300 mm. The adjustment of trim-cut width and replacement edge distance is enabled by the infeed axes (Y, y) with a movement range of 100 mm. All four axes are fast, precise, and dynamic (Aerotech PRO165LM: v_{max}: 2 m/s, bidirectional repeatability ± 1 μm, a_{max}: 30 m/s^2).

Figure 16 shows the arrangement of both *x*/*y* tables which are placed on a granite. The granite consists of a solid block and a demountable granite bridge to mount a manual *z*-axis for different laser processing heads or optional equipment like a positioning camera. The dimensions of the granite block are $860 \times 900 \times 250\,\text{mm}^3$ (width, depth, and height), and the bridge is 650 mm high and has a cross section of 100 mm^2. The granite with a weight of 450 kg is chosen to minimize mechanical vibrations.

The process area is in front of the bridge. To avoid damage due to laser radiation, spatters, and melt, there is an aperture in the granite underneath the process area (Fig. 17). Furthermore, that aperture enables diagnostics of melt flow and dross formation by means of a high speed camera from the bottom side. The granite is mounted on a sturdy steel frame. Three flexible supports are used to enable a precise horizontal and vertical alignment.

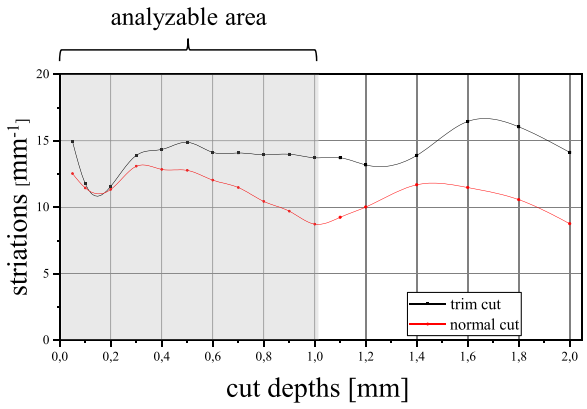

FIG. 14. Striations in relation to cut depths from top of a normal cut or a trim-cut for parameter set C.

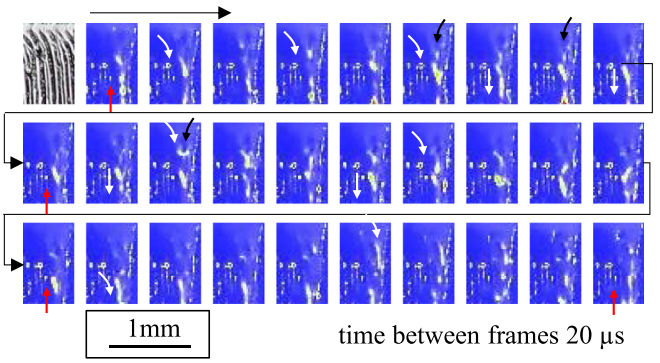

FIG. 15. Extract of high speed observation trim-cut frame series of trim-cut parameter set C, $z_F = -6$ mm.

Both *x*/*y* tables are precisely aligned in such a manner that the angular error along the movement distance of 300 mm is lower than 5 μm. Consequently, the trim-cut width and the distance between the replacement edge and the sample remain constant during the experiment. Thus, the distance between the cutting edge and the replacement edge can be minimized without collision of both elements. Trim-cuts with a distance lower than 25 μm are possible.

In order to be able to use macroobjectives with diameters up to approximately 75 mm, it is necessary to locate the replacement edge in a higher position than the surface of the *x*/*y* table; otherwise, the optical axis of the objective cannot be centered in the area of observation. Therefore, both *x*/*y* tables were placed with a height offset of 45 mm (Fig. 18).

Furthermore, a positioning camera (resolution <5 μm) is mounted laterally, off-axis to the processing area. This camera allows a precise adjustment of the trim-cut width and the replacement edge distance (Fig. 19).

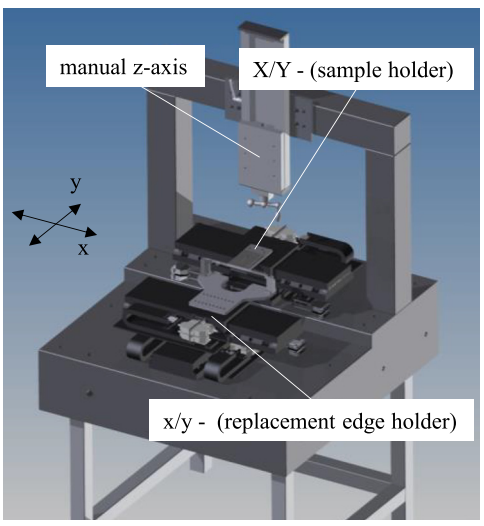

FIG. 16. Layout of advanced trim-cut test bench.

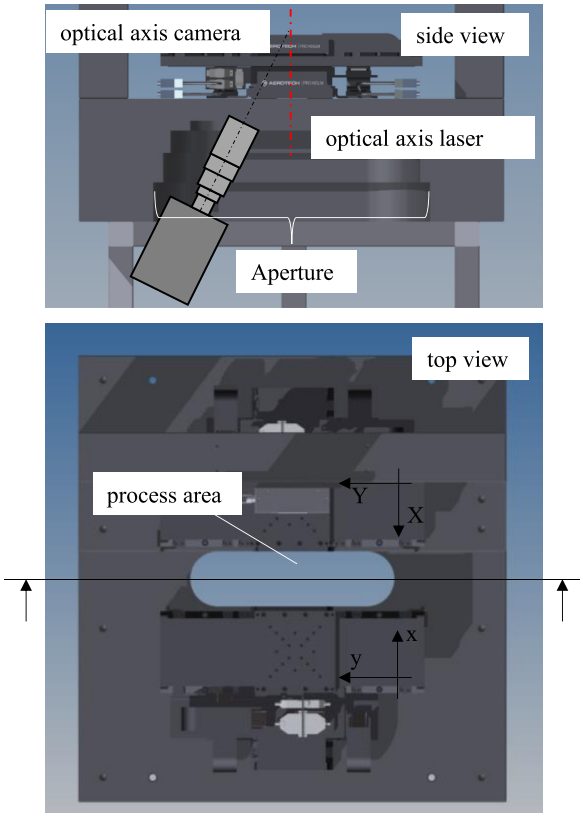

FIG. 17. Layout of advanced trim-cut test bench (side and top view).

2. Advanced trim-cut procedure

The purpose of the trim-cut procedure is to receive an analyzable high speed video of the striation generation on the cutting flank. Furthermore, it is useful to compare the trim cut flanks with normal cut flanks. Therefore, a trim-cut test set consists of a pre-cut, the trim-cut, an incomplete cut, and two complete cuts as described in Sec. III (cf. Fig. 8).

The pre-cut is used to measure the kerf width and calculate the positioning offset between the laser beam axis and the positioning camera by means of the absolute position coordinates of the *x*/*y* table. Thus, it is possible to adjust online the trim-cut width and the replacement edge distance below the positioning camera. By recalculating the positioning offset, the trim-cut can be performed below the cutting head with the adjusted values.

The incomplete cut and the two complete cuts are used to control the kerf width again and to get a sample with a left and right cut flank.

Furthermore, the trim-cut test bench enables a controlled infeed movement during the trim-cut by the two independent

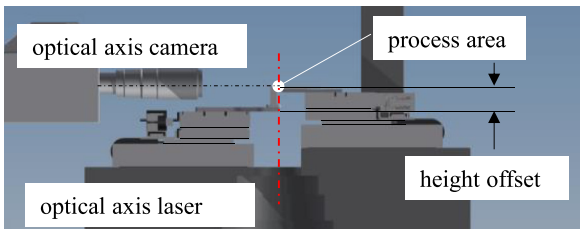

FIG. 18. Side view of advanced trim-cut test bench.

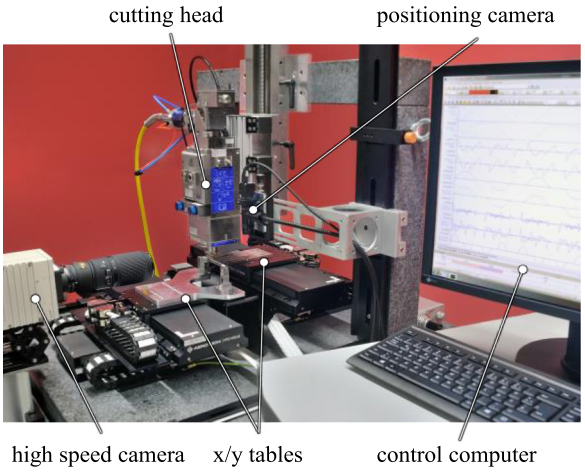

FIG. 19. Advanced trim-cut setup.

x/*y* tables. Thus, the trim-cut width and the replacement edge distance can be varied and adjusted during the trim-cut procedure.

In summary, it is possible to carry out systematic parameter series with this semiautomated trim-cut test bench. *In-situ* observation of the cutting process will deliver important insights regarding the dynamic characteristics of the melt flow and the resulting formation of striations and dross. The experimental findings will also serve to stimulate and verify advanced process models and stimulations.

IV. SUMMARY AND OUTLOOK

This work is focused on the observation of fluid dynamics of the laser cutting process by means of the trim-cut technique. First of all, a comprehensive review of hitherto existing trim-cut studies is given revealing the power of this method.

Again orienting trim-cuts with a fixed replacement edge are performed to reassess the trim-cut procedure itself and to clarify the requirements for the design of an advanced test bench. Ambitious targets regarding accuracy, reproducibility, and functionality lead to the engineering of a semiautomated system in order to enable systematic process investigations.

The resulting advanced trim-cut test bench consists of two fast, highly accurate and dynamic *x*/*y*-tables and versatile control features allowing semiautomated trim-cut series for a broad spectrum of laser beam cutting processes—from high speed to heavy section. The understanding of process dynamics is essential to find new techniques for improving process efficiency and quality. Test benches like the one described here can contribute.

In conclusion, the trim-cut procedure enables the temporal and spatial observation of the melt flow on the cutting front. Applying the advanced trim-cut test bench with the movable replacement edge, a further increase of the observation quality by means of the trim-cut procedure will be given.

ACKNOWLEDGMENTS

All presented investigations were conducted in the context of the Collaborative Research Centre SFB1120 “Precision

Melt Engineering" at RWTH Aachen University and funded by the German Research Foundation (DFG). The authors wish to express our sincere gratitude for the sponsorship and the support.

[1]D. A. Belforte, "2015 industrial laser market outperforms global manufacturing instability: Fiber Laser sales continue to drive growth," in *Industrial Laser Solutions for Manufacturing* (PennWell, Nashua, 2016), pp. 6–11.
[2]Y. Arata, H. Maruo, I. Miyamoto, and S. Takeuchi, "Dynamic behavior in laser gas cutting of mild steel," Trans. Jpn. Weld. Res. Inst. **8**, 175–186 (1979).
[3]H. Zefferer, D. Petring, W. Schulz, F. Schneider, and G. Herziger, "Laser beam fusion cutting: Diagnostics and modelling of melt drag and ripple formation," in *Laser in Engineering*, edited by W. Waidelich (Springer-Verlag, Berlin, Heidelberg, 1993), pp. 574–579.
[4]D. Petring, P. Abels, E. Beyer, and G. Herzinger, "Werkstoffbearbeitung mit Laserstrahlung, Teil 10: Schneiden von metallischen Werkstoffen mit CO_2-Hochleistungslasern," Feinwerk und Messtechnik **96**, 364–372 (1988).
[5]H. Zefferer, D. Petring, and E. Beyer, "Investigations of the gas flow in laser beam cutting," in *Strahltechnik. 135: Vorträge und Posterbeiträge der 3. Internationalen Konferenz "Strahltechnik" in Karlsruhe am 13. und 14. März 1991 = Beam technology* (Dt. Verl. für Schweißtechnik DVS-Verl, Düsseldorf, 1991), pp. 210–214.
[6]T. Fushimi, H. Horisawa, S. Yamaguchi, N. Yasunaga, and T. Fujioka, "Fundamental study of laser cutting using high-speed photography," Proc. SPIE **3888**, 90–95 (2000).
[7]P. V. Yudin, A. P. Petrov, and O. B. Kovalev, "Experimental modeling and high speed photographic studies of gas laser cutting of sheet metal," Proc. SPIE **6279** (2007).
[8]P. V. Yudin and O. Kovalev, "Visualization of events inside kerfs during laser cutting of fusible metal," in ICALEO 2007 Congress Proceedings, Orlando, FL (2007), pp. 772–779.
[9]P. V. Yudin and O. Kovalev, "Visualization of events inside kerfs during laser cutting of fusible metal," J. Laser Appl. **21**, 39–45 (2009).
[10]G. Ermolaev, P. V. Yudin, E. Verna, and T. Jouanneau, "Visualization and modeling of combustion effects at laser cutting of mild steel with oxygen," in Proceedings of Pacific International Conference on Applications of Lasers & Optics (Wuhan, China, 2010).
[11]D. Petring, "More about laser cutting - A mature laser application still has something up its sleeve," LIA Today **19**, 6–7 (2011).
[12]K. Hirano, "Study on striation generation process during laser cutting of steel," PhD thesis (Arts et Métiers ParisTech, Paris, 2012).
[13]P. V. Yudin, A. V. Zaitsev, O. B. Kovalev, and G. V. Ermolev, "Visualization and analysis of laser cutting of mild and stainless steel with Fiber and CO_2 lasers," in Proceedings of LAMP 2013 - The 6th International Congress on Laser Advanced Materials Processing, 2013.
[14]P. V. Yudin, A. V. Zaitsev, O. B. Kovalev, and G. V. Ermolev, "Fundamental study of CO_2- and Fiber laser cutting of industrial materials with high speed visualization technique," in Proceedings of LANE 2014.
[15]F. Tenner, B. Berg, C. Brock, F. Klämpfl, and M. Schmidt, "Experimental approach for quantification of fluid dynamics in laser metal welding," J. Laser Appl. **27**, S29003 (2015).

Meet the Author

Dennis Arntz is a PhD student at RWTH Aachen University in Germany. His research focusses on the improvement of laser-based cutting processes using high-speed imaging. He received his Bachelor of Science in Mechanical Engineering at RWTH Aachen University in 2012. In 2014 he obtained his master's degree in Development and Design. The master thesis contained different laser machining processes for the manufacturing specific design of a lightweight battery pack housing.